2024 IEEE International Conference on Systems, Man, and Cybernetics (SMC)
October 6-10, 2024. Sarawak, Malaysia

Towards 3D-Denser Ultrasound Image Simulation from 2D CT-Scan for Ultrasound-guided Percutaneous Nephrolithotomy Training

Sathiyamoorthy Selladurai[1], Ben Sainsbury[2], James Watterson[3], Rebecca Hibbert[4], Anila Satheesh B[5], Arun K. Thittai[5] and Carlos Rossa[1]

***Abstract*— Virtual reality (VR) simulation can improve the outcomes of percutaneous nephrolithotomy (PNCL) - a surgery to extract kidney stones using ultrasound (US) or fluoroscopy image guidance. These simulators almost exclusively employ fluoroscopy, and no commercial VR simulator is available for US-guided PNCL (usPCNL). In this paper, we proposed the first step towards developing an usPCNL simulator that integrates a volumetric US model of the patient's anatomy derived from parallel 2D computed tomography (CT) scans.**

A critical challenge in US image generation from CT scans is that the limited spatial resolution of CT slices may lead to inaccuracies in the simulated US images. The proposed algorithm interpolates successive CT images to create an augmented dataset with increased spatial resolution. Each CT slice is then converted into a US image based on principles of linear acoustics and spatial impulse response. These images are then combined to form two different volumetric US images, one derived from the original sparse CT scans, and one created with the augmented data. From these volumetric US images, new images can be formed along arbitrary imaging planes not captured in the original CT data. The obtained simulated images are compared with their corresponding real US images acquired experimentally, and further evaluated quantitatively using normalized root mean square error (NRMSE) and dice similarity coefficient (DSC). The results reveal an NRMSE of 0.235 ± 0.051 and a DSC of 0.9139 ± 0.062, showcasing a close resemblance between simulated and actual ultrasound images. Additionally, we show that denser CT scan data leads to a 25% improvement in image quality based on peak signal-to-noise ratio compared to the original dataset. This initial work is laying the foundation for the development of the usPCNL simulator, which could potentially have significant benefits for training and enhancing skills in this medical procedure.

I. INTRODUCTION

Percutaneous nephrolithotomy (PCNL) is the surgical standard to treat large ($> 2\,\text{cm}$) or complex renal calculi. During PCNL, access to the kidney is established through a percutaneous tract in the back or side which enables passage of a nephroscope used to visualize, fragment, and remove the kidney stones. Accurate puncture through the papilla of the desired calyx, to create percutaneous access for stone disintegration and removal, is essential. Preoperative computed tomography (CT) imaging is required to identify anatomical relationships to the kidney and to plan a trajectory for percutaneous access. Fluoroscopy or ultrasound image guidance is used intraoperatively to establish percutaneous access to the kidney. Despite being a common minimally invasive urological procedure, PCNL has a steep learning curve and is associated with a risk of complications such as bleeding, renal pelvis perforation, and risk of injury to surrounding organs, such as colon and spleen [1]. Real time biplanar fluoroscopy is the most frequently used technique for percutaneous puncture. However, fluoroscopy imaging is disadvantaged due to radiation exposure and single-plane imaging, and it does not provide visibility of adjacent organs such as the pleura and bowels, posing a risk of accidental injury. Ultrasound-guided PCNL (usPCNL) has several advantages over fluoroscopy owing to its non-ionizing nature, low cost, and higher frame rate. Ultrasound offers a clearer delineation of adjacent structures including the anterior and posterior calyces [2]–[4]. Despite these benefits, the adoption of usPCNL has been limited in North America, primarily due to the lack of training opportunities [19]. In addition, usPCNL requires an advanced skill level to interpret the ultrasound images, and identify the guide-wire and adjacent anatomical structures, while simultaneously coordinating the hand steering the wire and the hand maneuvering the ultrasound probe [13], [14]. Medical education increasingly relies on simulation-based training that accurately replicates such procedures [3], [5]. Prior research has explored various simulators for PCNL, spanning physical models to virtual reality environments [6]–[8]. However, existing solutions are mostly based on fluoroscopy and no virtual reality simulator has been proposed for usPCNL, mainly due to the prevalence of fluoroscopy use [9]–[12]. Some of these simulators, such as Marion Surgical's PCNL trainer [3], [4] convert preoperative CT images into a 3-dimensional (3D) model that is imported into the simulator, allowing urologists to practice the procedure on patient-specific data before entering the operating room [17], [18]. To develop an equivalent usPCNL simulator that leverages the same existing set of preoperative data, methods to simulate volumetric ultrasound images from existing sparse 2D CT scans are needed [15], [16].

Ultrasound image simulation from CT has garnered signif-

We acknowledge the support of the Natural Sciences and Engineering Research Council of Canada (NSERC), [funding ref. number ALLRP 580714-22]. Cette recherche a été financée par le Conseil de recherches en sciences naturelles et en génie du Canada (CRSNG), [no. de référ. ALLRP 580714-22].

[1]S. Selladurai and C. Rossa are with the Department of Systems and Computer Engineering, Carleton University, Ottawa, Ontario, Canada. selladurai.sathiyamoo@carleton.ca; rossa@sce.carleton.ca

[2]B. Sainsbury is with Marion Surgical, Seguin, Ontario, Canada. ben@marionsurgical.com

[3]J. Watterson is with the Faculty of Medicine, Division of Urology, University of Ottawa, Ottawa, ON, Canada. jwatterson@toh.ca

[4]R. Hibbert is with the Department of Radiology, Mayo Clinic, Rochester, MN, USA. hibbert.rebecca@mayo.edu

[5]A. Satheesh B and A. K. Thittai are with the Indian Inst. of Technology Madras, Chennai, India. ic39312@imail.iitm.ac.in; akthittai@iitm.ac.in

2024 IEEE International Conference on Systems, Man, and Cybernetics (SMC) | 978-1-6654-1020-5/24/$31.00 ©2024 IEEE | DOI: 10.1109/SMC54092.2024.10831528

icant attention in recent years [19]–[25]. Hostettler et al. [20] proposed a low-cost ultrasound simulator for ultrasonography training. Their method combines texture images derived from CT scans with echo maps and absorption images to simulate ultrasound images. However, their approach lacks speckle information. Burger et al. [21] simulate an ultrasound model of the tissue based on CT characteristics by propagating rays through beamforming and backscattering. Reichl et al. [22] use parallel programming for real-time simulation of ultrasound images. Karamalis et al. [23] model ultrasound wave propagation in tissue using the Westervelt equation via a finite difference scheme for real-time simulation. Even though various methodologies have been proposed for simulating ultrasound from CT images, most lack realism, accurate depth perception, and versatility in training scenarios [24], and are often limited to 2D images [21]. A critical challenge in ultrasound image simulation from CT scans is the limited spatial resolution of CT slices, which may lead to inaccuracies in the simulated ultrasound images. In this case, image interpolation techniques may be used to augment the dataset, resulting in denser and more comprehensive CT data. This enhancement may allow for a more accurate representation of tissue structures in the corresponding simulated ultrasound images.

To address this challenge, the development of realistic simulation platforms is imperative for training healthcare professionals effectively. In this paper, an approach for volumetric ultrasound image simulation from 2D CT scans, aimed at enhancing the realism and effectiveness of PCNL training simulators is presented.

This paper addresses the first step towards creating a usPCNL simulator by generating a volumetric ultrasound image from sparse 2D CT scans that can be sliced along any arbitrary imaging plane. In our approach, firstly, parallel 2D CT scan slices are interpolated to augment the dataset, resulting in denser and higher-resolution CT data. From each slice in the augmented dataset, a scattering map with normally distributed strength is created. Simulations are based on the principles of linear acoustics and computation of the spatial impulse response. Speckle is simulated by randomly placed scatterers with strength randomly chosen from a normal distribution. The Tupholme-Stepanishen method is then used for calculating pulsed ultrasound fields for both the pulsed and continuous wave cases for different transducers, from which the corresponding ultrasound image is created. These simulated 2D ultrasound images are arranged in a denser 3D voxel, thereby extending data formation to include CT slices not captured in the original dataset. Finally, we show that from the volumetric image, a 2D ultrasound image can be created along an arbitrary imaging plane and displayed in real-time.

To validate the concept, a set of CT scans and the corresponding ultrasound images are acquired from a phantom tissue. The simulated ultrasound images are compared with the real images. The results reveal that using denser CT scans leads to better-quality ultrasound images. The creation of 3D volumetric ultrasound datasets opens up possibilities for simulating images in directions that were not originally captured in the CT scans. This advancement is a crucial first step in the development of a realistic training simulator environment for usPCNL. Such a simulator would provide trainees with a more immersive and realistic experience, ultimately leading to improved proficiency and patient outcomes in usPCNL procedures. The paper is structured as follows: Section II elaborates on the methodology employed for simulating ultrasound images from CT, the formation of 3D ultrasound in section III, followed by the definition of image quality metrics used for comparison in Section IV. Section V presents the results, followed by a discussion on the implications and future prospects in Section VI.

II. VOLUMETRIC ULTRASOUND IMAGE SIMULATION FROM 2D CT SCANS

We consider having a set of parallel 2D CT scans obtained from a given tissue, as well as the corresponding ultrasound images acquired with a curvilinear transducer at the same location of each CT slice. Fig. 1 shows an overview of the methodology employed to create a dense volumetric ultrasound image from sparse 2D scans. First, bi-linear interpolation is used to interpolate two consecutive scans to augment the data. Each scan is individually converted into a 2D ultrasound image using a physics-based model. The simulated ultrasound images are then compared with their corresponding real images. The ultrasound images are then combined in a volumetric image, which allows new images to be generated along an arbitrary imaging plane. The following subsections describe each of these steps in greater detail.

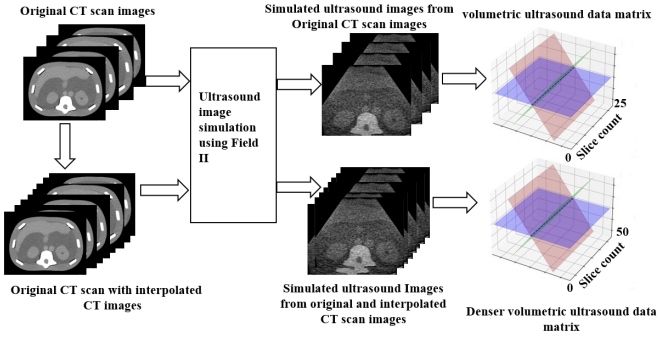

Fig. 1. Workflow to generate volumetric ultrasound images from 2D CT scans. In (a), sparse 2D CT scans are interpolated to improve spatial resolution. (b) displays the simulated ultrasound images generated from each CT slice. (c) shows the ultrasound volumetric data formed from the original CT data. The interpolated CT set then follows the same workflow in (d), (e), and (f). The use of interpolated CT slides leads to improved volumetric ultrasound images along an arbitrary imaging plane.

A. CT Images Pre-processing

Since CT slices are rectangular and have a much larger area than the curvilinear ultrasound images, the first step in the algorithm is to specify a region of interest in each CT slice. This region of interest (ROI) corresponds to the imaging plane of the ultrasound transducer. For PCNL, we consider a curvilinear ultrasound transducer with a width of

60 mm and a fixed penetration depth of 180 mm. Thus, the ROI is a sector image at the centre of the slice with a radius of 180 mm. This sector image, which is in cartesian coordinates, is remapped to a rectangle image by doing polar to Cartesian conversion as done in Fig. 2(a).

The trapezoidal ROI image is then transformed into a rectangular image using polar-to-Cartesian conversion, see Fig. 2(b)-(c). This is done for two reasons: 1) Converting the ROI image shape to a rectangle allows for the application of the same simulation method to both linear and curvilinear array transducers, and 2) the pixel spacing in CT images is usually higher than the ultrasound signal wavelength. To transform the trapezoidal ROI image into a rectangular image using polar-to-Cartesian conversion, we need to map each pixel from the polar coordinate system of the trapezoidal ROI to the Cartesian coordinate system of the rectangular image. This transformation involves converting the radial distance r and angular position θ of each pixel to Cartesian coordinates (x, y) as follows:

$$x = r\cos(\theta), \qquad y = r\sin(\theta) \tag{1}$$

where x and y are is the horizontal and vertical coordinates of the pixel in the rectangular image, r is the radial distance from the origin to the pixel in the trapezoidal ROI, θ is the angle in radians from a reference axis to the pixel in the trapezoidal ROI. These equations allow us to express any pixel in the trapezoidal ROI image in terms of its Cartesian coordinates (x, y) in the rectangular image, effectively transforming the shape from a trapezoid to a rectangle. To perform the reverse process, converting rectangular coordinates (x, y) back to polar coordinates (r, θ), we use:

$$r = \sqrt{x^2 + y^2}, \qquad \theta = \arctan\left(\frac{y}{x}\right) \tag{2}$$

where $\sqrt{x^2 + y^2}$ calculates the Euclidean distance from the origin to the point, giving the radial distance r and atan2 $\left(\frac{y}{x}\right)$ calculates the angle θ using the *atan2* arctangent function, taking into account the signs of x and y to determine the correct quadrant. Following this step, to generate high-quality volumetric ultrasound images from sparsely acquired 2D CT images, the ROI of two consecutive images is interpolated to create new images between the two samples using a straightforward bilinear interpolation [1]. Given two consecutive original 2D slices, new slices are generated by interpolating pixel values between them. This process involves generating intermediate slices between the original ones to increase the density of the volume. One common method, bilinear interpolation, calculates pixel values for the new slices based on those of the neighbouring pixels in the original slices. Given a point (x, y) in the new slice, the pixel value $f(x, y)$ can be interpolated from the surrounding two pixels (x_1, y_1), (x_1, y_2), (x_2, y_1), and (x_2, y_2) in the original slices:

$$\begin{aligned} f(x,y) =& (1-\alpha)(1-\beta)f(x_1,y_1) + \alpha(1-\beta)f(x_2,y_1) \\ &+ (1-\alpha)\beta f(x_1,y_2) + \alpha\beta f(x_2,y_2) \end{aligned} \tag{3}$$

where $\alpha = (x - x_1)/(x_2 - x_1)$ and $\beta = (y - y_1)/(y_2 - y_1)$.

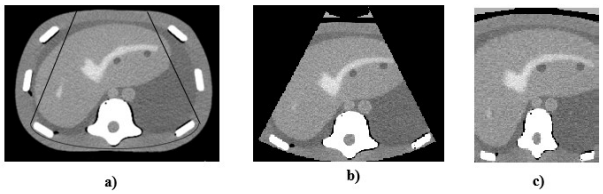

Fig. 2. Images showing the input CT slice from a phantom. The region of interest is marked with a black solid line in (a). The ultrasound transducer is assumed to be at the center of the slice. The region of interest extracted from CT is shown in (b), before it is converted into a rectangular image in (c).

B. 2D Ultrasound Simulation

Ultrasound image simulation from CT data is performed across all interpolated and original axial CT slices, assuming the transducer is consistently positioned at the center of each slice. The anatomies of the tissue's ultrasound images scattering strength of the region of interest is created. This map then determines the factor multiplied by the scattering amplitude generated from a Gaussian distribution. Currently, the elevation direction is made by making a 15 mm thickness for the scatter positions, which are randomly distributed in the interval. The simulations are done by simulating and summing the field from a collection of point scatterers. A single RF line in an image can be calculated by summing the responses from a collection of scatterers. The final simulated image consists of 128 RF(radio frequency) lines with 0.7 degrees between lines. This is then interpolated to form the B-mode ultrasound image using principles of linear acoustics to generate ultrasound images based on tissue characteristics derived from CT scans as follows:

Scattering Map Generation with Boundaries: First, a bitmap image representing the scattering strength of the region of interest (ROI) is created. This map determines the factor multiplied by the scattering amplitude generated from a Gaussian distribution, modelling the density and speed of sound perturbations in the tissue. Simulated boundaries are introduced by defining lines in the scatterer map along which strong scatterers are placed. This step enhances the realism of the simulated ultrasound images.

Random Scatterer Distribution and Field Simulation: Next, a large number of scatterers (e.g., 1,000,000) are randomly distributed within the ROI. The scatter amplitude and standard deviation are determined by the scattering map, ensuring variability in scatterer properties. Then, we calculate and sum the acoustic pressure field $p(x, y, z, t)$ resulting from this collection of point scatterers at a point in space and time (x, y, z) at time t as

$$p(x,y,z,t) = \sum_{i=1}^{N} A_i e^{-j2\pi \frac{f_0}{c}\sqrt{(x-x_i)^2+(y-y_i)^2+(z-z_i)^2}} \tag{4}$$

where N is the number of scatterers, A_i is the amplitude of the i^{th} scatterer, f_0 is the center frequency of the transducer, c is the speed of sound in the medium, and (x_i, y_i, z_i) are the coordinates of the i^{th} scatterer. The resulting acoustic

pressure field mimics the behaviour of ultrasound waves propagating through tissue. The sum represents the contribution of each scatterer to the overall acoustic pressure at a given point.

Calculation of Scattering Strength: The scattering strength of each scatterer can be determined based on the tissue properties at its location. Let's denote the scattering strength as σ_i for the i^{th} scatterer. This can be calculated using a scattering map $S(x, y)$ as follows:

$$\sigma_i = S(x_i, y_i) \tag{5}$$

where (x_i, y_i) are the coordinates of the i^{th} scatterer.

Gaussian Distribution of Scatter Amplitude: The scatter amplitude A_i of each scatterer can be randomly chosen from a Gaussian distribution with mean μ_i and standard deviation σ_i. This ensures variability in scatterer properties, mimicking the natural variations in tissue characteristics. The amplitude of the i^{th} scatterer is given by:

$$A_i \sim \mathcal{N}(\mu_i, \sigma_i) \tag{6}$$

where $\mathcal{N}(\mu_i, \sigma_i)$ represents a Gaussian distribution with mean μ_i and standard deviation σ_i.

Calculation of RF Line: To calculate a single RF line in the ultrasound image, the responses from a collection of scatterers are summed. Let us denote the RF line signal at depth z as $s(z)$. This can be calculated by summing the contributions from all scatterers within the four imaging plane:

$$s(z) = \sum_{i=1}^{N} A_i e^{-j2\pi \frac{f_0}{c} \sqrt{(x_i - x_c)^2 + (y_i - y_c)^2 + z^2}} \tag{7}$$

where (x_c, y_c) are the coordinates of the transducer center, f_0 is the center frequency of the transducer, and c is the speed of sound in the medium.

Interpolation for B-Mode Ultrasound Image: The final simulated ultrasound map consists of multiple RF lines. Each RF line is calculated by summing the responses from a collection of scatterers. Once the RF lines are calculated, they are interpolated to form the B-mode ultrasound image. Bilinear interpolation is commonly used for this purpose. Given the RF lines at discrete depth intervals, new RF lines at intermediate depths are generated by interpolating the values between adjacent RF lines.

These equations implemented using the Field II MATLAB toolbox, enable the simulation of realistic ultrasound images can be simulated from the original CT data. The next step is to combine the created 2D ultrasound images to form a volumetric image, from which new images can be created along arbitrary imaging places not originally captured by the CT scans.

III. 3D ULTRASOUND SIMULATION

Once the ultrasound images are generated, they are stacked together along the z axis to form a 3D voxel. Each voxel element contains the pixel values corresponding to a particular location in the tissue volume. The density of the voxel increases with the number of interpolated slices, resulting in a denser representation of the tissue.

Given a set of 2D ultrasound images, $I_i(x, y)$ where $i = 1, 2, ..., N$, each representing a cross-sectional view, a 3D ultrasound volume $V(x, y, z)$ can be constructed by stacking these images along the z-axis:

$$V(x, y, z) = \sum_{i=1}^{N} I_i(x, y) \cdot \delta(z - z_i) \tag{8}$$

where z_i represents the z-coordinate of the i^{th} image plane, and δ is the Dirac delta function. To form a 2D slice from the 3D voxel along a different imaging plane, a process called slicing is performed. Slicing involves selecting a plane within the 3D volume and extracting the pixel values along that plane. This can be achieved by specifying the orientation and position of the plane relative to the voxel grid.

The next step is to extract a 2D slice from the 3D voxel along a given imaging plane, which we define by vector $\mathbf{n}$ normal to that plane, whose tail is at (x_0, y_0, z_0). If (x, y, z) is any point on the plane, then the vector $\langle x - x_0, y - y_0, z - z_0 \rangle$ lies entirely inside the plane and so must be perpendicular $\mathbf{n}$, that is,

$$\mathbf{n} \cdot \langle x - x_0, y - y_0, z - z_0 \rangle = 0 \tag{9}$$

If n_x, n_y, n_z are the components of $\mathbf{n}$, then

$$n_x(x - x_0) + n_y(y - y_0) + n_z(z - z_0) = 0 \tag{10}$$

or rather:

$$n_x x + n_y y + n_z z = d \tag{11}$$

where $d = n_x x_0 + n_y y_0 + n_z z_0$. Once the plane is defined, it can be discretized into pixels that take the value of the closest pixel in the 3D volume. After all pixels on the plane are populated, the resulting 2D image from the 3D voxel can then be interpolated using (3).

IV. PERFORMANCE METRICS

In the field of image analysis and pattern recognition, evaluating the similarity between two images is a fundamental task. Once ultrasound images are generated from CT slices, performance metrics can be defined to compare the quality of the simulated ultrasound images against the ground-truth ultrasound images acquired at the same location as the input CT scan. Three performance metrics will be used.

1) Normalized Root Mean Square Error (NRMSE): NRMSE, is a dimensionless metric used for comparing an image with a reference image, calculated as:

$$\text{RMSE} = \sqrt{\frac{1}{M \cdot N} \sum_{m=1}^{M} \sum_{n=1}^{N} \frac{\left[I_{in}(m, n) - I_{ref}(m, n)\right]^2}{I_{max} - I_{min}}} \tag{12}$$

where m and n are the vertical and horizontal coordinates of a given pixel, and I_{in} and I_{ref} represent the input and reference images, respectively, with dimensions $M \cdot N$, and I_{max} and I_{min} denote the maximum and minimum pixel values in the images, set to 1 and 0, respectively.

2) Dice Similarity Coefficient (DSC): DSC is a widely used metric for measuring similarity between two images. The DSC is defined as the ratio of twice the intersection of two sets to the sum of the cardinalities of the two sets. In the context of image segmentation, it quantifies the agreement between the segmented regions and ground truth as

$$\text{DSC} = \frac{|X| + |Y|}{2|X \cap Y|} \tag{13}$$

where X and Y represent the sets of pixels in the segmented region and ground truth, respectively, and $|X|$ and $|Y|$ denote the cardinalities of sets X and Y, respectively. The DSC is compared between the ground truth ultrasound image obtained experimentally and simulated ultrasound images.

3) Peak signal-to-noise ratio (PSNR): To evaluate how denser data improves volumetric ultrasound image simulation, PSNR is computed between two equivalent 2D ultrasound images taken from each volumetric image. The PSNR in decibels between two images is used as a quality measurement between the image slice taken from volumetric data created from sparse CT data, and the corresponding image slice taken from the volumetric ultrasound image simulated with augmented, interpolated CT slices along the same random imaging plane. The higher the PSNR, the better the quality of the reconstructed image. It can be calculated as:

$$PSNR = 10 \log_{10} \left(\frac{R^2}{\epsilon} \right) \tag{14}$$

where R is the maximum fluctuation in the input image data, and ϵ is the mean square error

$$\epsilon = \frac{\sum_{M,N} [I_1(m,n) - I_2(m,n)]^2}{M \times N}. \tag{15}$$

in which M and N are the number of rows and columns in the input image, respectively. While both the mean-square error and PSNR are used to compare image compression quality, the mean-square error represents the cumulative squared error between the compressed and original image.

V. RESULTS AND DISCUSSION

A set of 2D ultrasound images and the corresponding 2D CT scans are acquired from a triple imaging modality abdominal phantom (from CIRS, Model 057A), measuring 26 cm x 12.5 cm x 19 cm, which accurately represents an adult abdomen and is compatible with CT, ultrasound, and MRI imaging modalities. Its internal structures include the liver, partial lung, portal vein, two partial kidneys, abdominal aorta, vena cava, simulated spine, and six ribs, along with eight lesions. Ultrasound images of the phantom were acquired using a SONIX TOUCH Q+® scanner (Ultrasonix, Analogic Corporation, Peabody, MA, USA). These ultrasound images serve as the ground truth for comparison with ultrasound images simulated from CT data using Field II.

CT images of the phantom are acquired with a spacing of 1 mm and thickness of 1.25 mm. To realize a denser volumetric ultrasound simulator, the 1 mm spacing between the slices is further reduced to 0.5 mm using the interpolation described earlier. To this end, 25 axial CT slices were chosen from the database and subjected to pre-processing. Bilinear interpolation was employed between each pair of adjacent slices to generate an additional slice in between. This process was repeated for every pair of adjacent slices, resulting in the generation of another 25 CT slices. This augmented dataset provides denser, higher volumetric data. These original and interpolated CT data are further used for simulating ultrasound data, which is then used for forming a volumetric simulator for PCNL training purposes.

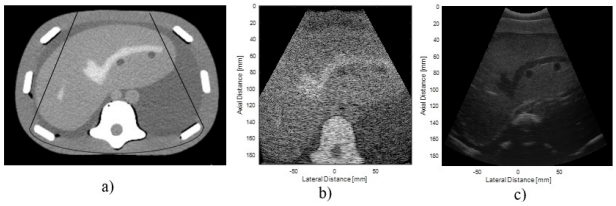

Fig. 3. Comparison between (a) ground-truth CT slice with chosen sector ROI marked with a black solid line, (b) ultrasound image generated through Field II, and (c) ground-truth ultrasound image that was acquired experimentally.

In the simulation, the transducer array is positioned at the centre of an axial CT slice, and a curvilinear transducer C2-5 is utilized with specifications outlined in Table 1. The depth of ultrasound signal penetration in both original database images is standardized at 180 mm.

TABLE I
PARAMETERS USED FOR ULTRASOUND SIMULATION FROM CT SCANS.

Parameter	Value
Operating frequency	2.5 MHz
Bandwidth	2-5 MHz
Transducer element pitch	0.47 mm
Number of elements	128
Speed of sound	1540 m/s
Sampling frequency	40 MHz

Fig. 3a shows an axial CT slice from the database. The chosen sector ROI within the CT slice is marked with a black solid line. The anatomy of the ROI consists of a top fat layer (dark), muscle layer (slightly brighter than fat), liver with two lesions (dark round circles) and hepatic vein, vertebra (bright region), abdominal aorta, vena cava (two round regions above vertebra), and surrounding soft tissue (dark region) with a portion of kidney in them.

One can observe that the bone-tissue interface has the highest weighting. The ultrasound simulations do not account for attenuation, making bones visible. However, the difference between the two images is small, although in the reference image acquired experimentally the ultrasound attenuation is large in bones. Hence, the region below the bone-tissue interface is darker than the bone in the reference image. The images are compared quantitatively using normalized RMSE and DSC as metrics for 25 different axial CT slices (see Table II). Since the experimentally

TABLE II
PERFORMANCE METRICS FOR SIMULATION

Sl. no.	*Parameters*	*Reference vs simulated image*
1	NRMSC	0.235 ± 0.051
2	DSC	0.9139 ± 0.062

TABLE III
PERFORMANCE METRICS FOR VOLUMETRIC DATA

Sl.no	Parameter	Original Volume Data	Denser Volume Data
1	PSNR	18.013 ± 2.19	24.27 ± 2.56

obtained ultrasound image from the same ROI is available from ultrasound scanning of the phantom, the comparison is also made between the ultrasound images simulated from CT images and the ground truth ultrasound images (Fig. 3). Again, the results obtained show that the actual ultrasound and simulated ultrasound images are similar. All of the images are displayed at 60 dB dynamic range.

Two volumetric images were created. The first only includes the original 25 slices, whereas the second set includes the original slices and the additional 25 interpolated slices, for a total of 50 slides. Each volumetric image is then sliced along the same 10 arbitrary imaging planes, and the corresponding 2D image is created following the procedure described earlier. An example is seen in Fig. 4 for 3 of these planes. PSNR is computed between the corresponding image slices taken from each volumetric images to evaluate the improvement quantitatively. The results are tabulated in Table III. The higher the PSNR, the better the quality of the reconstructed image. The results show a 25% improvement in PSNR when using the denser volumetric image.

VI. CONCLUSION AND FUTURE WORK

In this paper, we proposed a method to generate volumetric ultrasound images from 2D CT scans, laying the groundwork for the creation of a virtual reality simulator tailored specifically for usPCNL. Our approach addresses the challenge of limited spatial resolution in CT scans by employing interpolation techniques to augment the dataset, resulting in denser and higher-resolution CT data. These augmented CT scans were then utilized to simulate ultrasound images based on principles of linear acoustics and spatial impulse response computation. Performance evaluation of our image generation algorithm using normalized RMSE, DSC, and PSNR demonstrates its effectiveness in accurately simulating ultrasound images from CT data. The comparison between simulated and ground-truth ultrasound images shows minimal differences, indicating high fidelity in our simulation. Our results also suggest that denser CT scan data led to a significant improvement in ultrasound image quality obtained along an imaging plane not captured in the original data.

The proposed method lays the foundation for the development of a realistic simulator for usPCNL training. By simulating volumetric ultrasound images from CT scans, our approach will enable trainees to practice usPCNL procedures on patient-specific data before entering the operating room, ultimately enhancing their skills and improving patient outcomes. Furthermore, the ability to generate ultrasound images along arbitrary imaging planes not originally captured in the CT scans expands the versatility and effectiveness of the simulator for training scenarios.

Our current approach focuses on simulating ultrasound images from static CT scans. Expanding this methodology

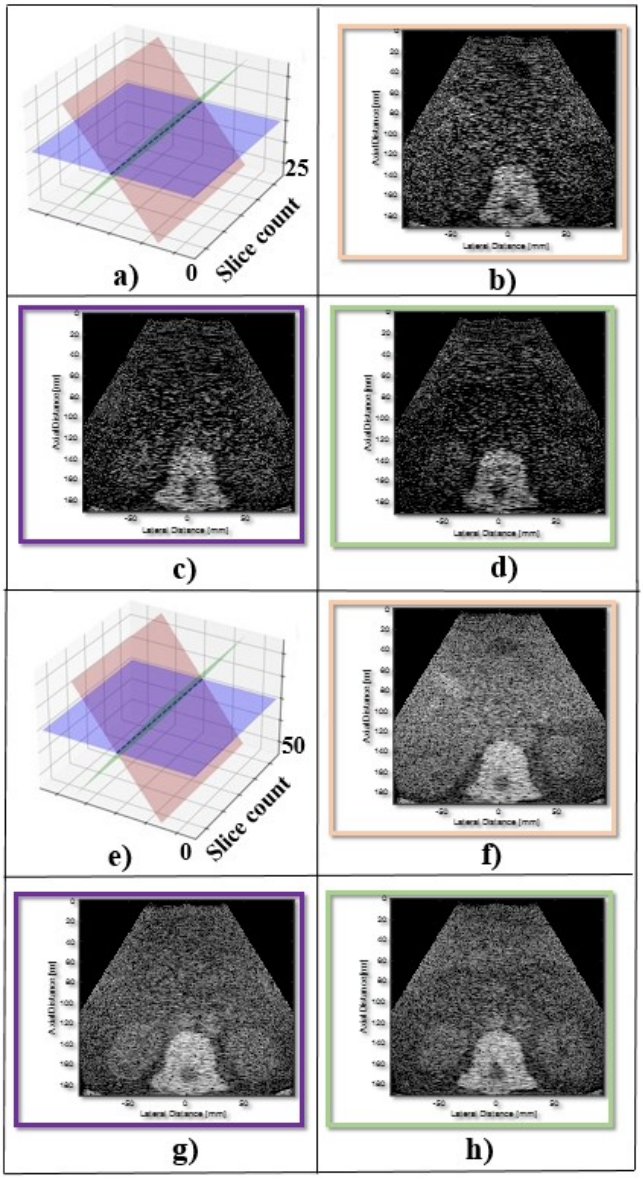

Fig. 4. (a) Shows ultrasound volumetric data formed from the original 25 CT slices, (b) Ultrasound image formed from the slice shown in orange in (a), (c) ultrasound image formed from the slice shown in blue in (a),(d) ultrasound image formed from the slice shown in green in (a), (e) denser ultrasound volumetric data formed from ultrasound images corresponding to 50 CT slices, (f) ultrasound image formed from the slice shown in orange in (e), (g) ultrasound image formed from the slice shown in blue in (e), and (h) ultrasound image formed from the slice shown in green in (e).

to incorporate dynamic anatomical changes, such as tissue deformation and organ motion, would further enhance the realism of the simulation platform. Furthermore, the scalability of our approach should be explored to accommodate variations in patient anatomy and pathology. Customization options tailored to individual patient cases would enable personalized training scenarios, catering to diverse clinical situations encountered in real-world practice. Lastly, collaborative efforts with medical educators and practitioners would be invaluable in refining the image-processing functionality and ensuring its alignment with training objectives and clinical standards. By incorporating feedback from experts in the field, we can iteratively improve the simulation platform to better serve the needs of trainees and ultimately contribute to improved patient outcomes in usPCNL procedures. Moreover, we intended to explore machine learning techniques to personalize training scenarios based on individual trainee performance and learning needs.

In conclusion, this preliminary work represents an important step towards the development of an ultrasound 3D volumetric framework for usPCNL training, which can ultimately improve patient outcomes and safety in clinical practice.

REFERENCES

[1] T. Tugcu, S. Yagci, E. Ozbek, et al., "Complications of percutaneous nephrolithotomy: A comprehensive review," *Journal of Endourology*, vol. 26, no. 8, pp. 1017-1023, 2012.

[2] J. Smith, A. Johnson, and B. Williams, "Ultrasound-guided percutaneous nephrolithotomy: A systematic review and meta-analysis," *Journal of Endourology*, vol. 34, no. 5, pp. 589–596, 2020.

[3] B. Sainsbury, M. Lacki, M. Shahait, M. Goldenberg, A. Baghdadi, L. Cavuoto, J. Ren, M. Green, J. Lee, T. D. Averch, et al., "Evaluation of a virtual reality percutaneous nephrolithotomy (PCNL) surgical simulator," *Front. Robot. AI*, vol. 6, p. 145, 2020.

[4] B. Sainsbury, O. Wilz, J. Ren, M. Green, M. Fergie, and C. Rossa, "Preoperative virtual reality surgical rehearsal of renal access during percutaneous nephrolithotomy: A pilot study," *Electronics*, vol. 11, no. 10, p. 1562, 2022.

[5] M. Maheu-Cadotte and R. Lee, "Advancements in simulation-based training: Meeting the growing need for realistic surgical simulators," *Journal of Medical Education*, vol. 45, no. 3, pp. 211–225, 2021.

[6] A. Johnson, J. Smith, and B. Williams, "A review of simulators for percutaneous nephrolithotomy training," *J. Endourology*, vol. 38, pp. 123–135, 2022.

[7] C. Garcia, D. Martinez, and E. Lopez, "Virtual reality simulators for percutaneous nephrolithotomy: A comparative study," *Simulation in Healthcare*, vol. 12, pp. 289–302, 2023.

[8] R. Patel, S. Jones, and M. Brown, "Physical models for percutaneous nephrolithotomy training: A systematic review," *Med. Education*, vol. 55, pp. 67–78, 2021.

[9] H. Lee, S. Kim, and J. Park, "Advancements in kidney anatomy replication for ultrasound-guided percutaneous nephrolithotomy simulators," *J. Med. Simulation*, vol. 20, pp. 210–225, 2023.

[10] L. Chen, Y. Wang, and M. Liu, "Integrating advanced imaging modalities into ultrasound-guided percutaneous nephrolithotomy simulators: A review," *Int. J. Comput. Assist. Radiol. Surg.*, vol. 15, pp. 1025–1038, 2022.

[11] Q. Wang, Z. Li, and W. Zhang, "Enhanced simulation techniques in ultrasound-guided percutaneous nephrolithotomy training," *J. Endourology*, vol. 40, pp. 55–68, 2023.

[12] A. Kumar, S. Gupta, and R. Sharma, "Recent advances in cyber-physical systems for medical simulation," *IEEE Trans. Biomed. Eng.*, vol. 68, pp. 789–802, 2022.

[13] H. Chen, L. Wang, and S. Zhang, "Advancements in biomedical ultrasound imaging for image-guided procedures," *IEEE Trans. Ultrason. Ferroelectr. Freq. Control*, vol. 67, pp. 820–835, 2020.

[14] J. Smith, A. Johnson, and B. Williams, "Challenges and opportunities in interpreting ultrasound images for image-guided procedures," *J. Med. Imaging*, vol. 28, pp. 415–428, 2021.

[15] Q. Wang, Z. Li, and W. Zhang, "Simulation of ultrasound images for workforce training in image-guided procedures," *J. Med. Simulation*, vol. 22, pp. 301–315, 2021.

[16] C. Garcia, D. Martinez, and E. Lopez, "Utilizing patient-specific preplanning data for simulation of ultrasound images in image-guided procedures," *Simulation Healthc.*, vol. 18, pp. 120–135, 2022.

[17] Smith, J., Johnson, A. "Utilizing CT Scan Data for Ultrasound Image Simulation in Percutaneous Nephrolithotomy." IEEE Transactions on Medical Imaging, 39(8), 2456-2462, 2022.

[18] J. Rotmensch, S.E. Waggoner, C. Quiet, "Ultrasound guidance for placement of difficult intracavitary implants", Gynecol. Oncol. 54 (1994) 159–162.

[19] A. Satheesh B. and A. K. Thittai, "A fast method for simulating ultrasound image from patient-specific CT data." Biomedical Signal Processing and Control, vol. 48, pp. 61–68, Elsevier, 2019.

[20] A. Hostettler, C. Forest, A. Forgione, L. Soler, J. Marescaux, Real-time ultrasonography simulator based on 3D CT-scan images, Stud. Health Technol. Inform. 111, 191–193, 2005.

[21] B. Burger, C. Abkai, Simulation of dynamic ultrasound based on CT models for medical education, Stud. Health Technol. Inform. 132 (2008) 56–61.

[22] T. Reichl, J. Passenger, O. Acosta, O. Salvado, Ultrasound goes GPU: real-time simulation using CUDA, Proc. SPIE (2009).

[23] A. Karamalis, W. Wein, N. Navab, "Fast Ultrasound Image Simulation Using the Westervelt Equation", In Int. Conference on Medical Image Computing and Computer-Assisted Intervention (2010), Springer, Berlin, Heidelberg, 2010, pp. 243–250.

[24] Yang, Y., et al. (2019). Ultrasound guided versus fluoroscopy guided percutaneous nephrolithotomy: a systematic review and meta-analysis. World Journal of Urology, 37(5), 777-788.

[25] A. Jensen, S. Nikolov, Fast simulation of ultrasound images, proceedings the IEEE Ultrasonics Symposium in Puerto Rico, October 2000.